Interacting chains of orbital polarons in the colossal magnetoresistance material $La_{1-x}Sr_xMnO_3$ revealed by spin and lattice dynamics

M. Hennion,[1,*] S. Petit,[1,†] A. Ivanov,[2,‡] D. Lamago,[3,1] and J. P. Castellan[3,1]

[1]*Laboratoire Léon Brillouin, CEA, CNRS, Université Paris-Saclay, F-91191 Gif-sur-Yvette, France*

[2]*Institut Laue-Langevin, 71 avenue des Martyrs, 38000 Grenoble, France*
and Peter the Great St. Petersburg Polytechnic University, 195251 St. Petersburg, Russia

[3]*Institut für Festkörperphysik, Karlsruher Institut für Technologie, D-76021 Karlsruhe, Germany*

(Received 6 April 2017; revised manuscript received 17 April 2019; published 10 June 2019)

The origin of the effect of "colossal magnetoresistance" (CMR) remains still unexplained. In this work we revisit the spin dynamics of the pseudocubic $La_{1-x}Sr_xMnO_3$ along the Mn-O-Mn bond direction at four x doping values ($x \leqslant 0.5$) and various temperatures and report a lattice dynamics study at $x_0 = 0.2$, representative of optimal doping for CMR. We propose an interpretation of the spin dynamics in terms of orbital polarons. This picture is supported by the observation of a discrete magnetic energy spectrum $E_n^{\rm mag}(q)$ with n levels, characteristic of the internal excitations of "orbital polarons" defined by Mn^{3+} neighbors surrounding a central Mn^{4+} hole. Because of its hopping, the hole mixes dynamically all the possible orbital configurations of its surrounding Mn^{3+} with degenerate energies. The $E_n^{\rm mag}$ values indicate a lifting of orbital degeneracy by phonon excitations. The n value and the q range are used to characterize these orbital polarons in direct space. At $x = 0.125$ and $x = 0.3$ the spectrum reveals two-dimensional polarons coupled by exchange and three-dimensional "free" polarons, respectively, with sizes $\ell = 1.67a \leqslant 2a$ in all bond directions. At $x_0 = 0.2$, the spin and the lattice dynamics provide evidence for chains of orbital polarons of size $\ell = 2a$ with a periodic distribution over $\approx 3a$ and an interaction energy ≈ 3 meV. At $T \leqslant T_c$ the charges propagate together with the longitudinal acoustic phonons along the chains enhancing their ferromagnetic character. The phase separation between metallic and ferromagnetic chains in a nonmetallic matrix may be crucial for CMR.

DOI: 10.1103/PhysRevB.99.214416

I. INTRODUCTION

In the rich variety of strongly correlated quantum materials [1–5], manganites are known for their "colossal" magnetoresistance properties (CMR). In these compounds, atomic substitution by various cations like Ca or Sr modifies the conduction properties, driving metallic behavior and CMR at an optimal doping x_0. These compounds are usually classified according to the width W of the electronic band, which can be defined depending on the existence of charge-ordered structures in the phase diagram [6]. Furthermore, spin, charge, lattice, and orbital interactions simultaneously active in these systems yield an intrinsic complexity resulting in inhomogeneous states [1]. The importance of such nanoscale magnetic inhomogeneities was early recognized, and observed close to the ferromagnetic and metallic phase transition at $T = T_c$ [7–9]. Phonon anomalies were also reported in the high-energy range [10–12]. The role of the "correlated lattice polarons" observed at $T \geqslant T_c$ has been highly debated [13–18]. However, how a magnetic field applied in such a state induces colossal magnetoresistance properties remains an issue. In this context, the study of spin dynamics has attracted a lot of attention. Below T_c, in all the compounds, the magnetic excitation spectrum is unconventional with a significant broadening and, in the metallic state, a softening of the spectra close to the zone boundary ($q = \pi/a$ where a is a pseudocubic lattice parameter) [19–24]. Their magnetic origin was demonstrated by polarized neutrons scattering studies [25]. In the compound $La_{1-x}Sr_xMnO_3$ with the largest electronic band [6] it was shown that the spin-wave broadening close to the zone boundary can be resolved into a series of n discrete modes [26,27]. In this paper they are called $E_n^{\rm mag}(q)$. Importantly, in the charge-ordered state observed at $x = 0.125$, $T \leqslant T_{o'o''}$ ($T_{o'o''} = 159$ K is the charge-ordering transition), the dispersion of the magnetic branches was found in coincidence with the phonon ones [28].

In this work, we revisit the spin dynamics of $La_{1-x}Sr_xMnO_3$ for several x doping values ranging from the quasimetallic to the metallic states [29] along the direction Mn-O-Mn of charge hopping [30]. There, $x_0 \sim 0.15$–0.2 [31]. In addition to the three compounds previously studied [26,27], namely, with $x = 0.125$ for $T > T_{o'o''}$, $x_0 = 0.2$, representative of the optimum doping for the CMR, and $x = 0.3$, we report a determination of the spin excitation spectrum at $x = 0.4$. On this basis, we propose a comprehensive analysis of the discrete spectrum as a function of doping within a unified picture in which all the degrees of freedom are simultaneously at play. We also determine the lattice excitation spectrum in the acoustic range for $x_0 = 0.2$, around T_c providing a complete picture of the magnetic and lattice excitations in the doping range of the optimal magnetoresistance doping value.

*martine.hennion@cea.fr
†sylvain.petit@cea.fr
‡aivanov@ill.fr

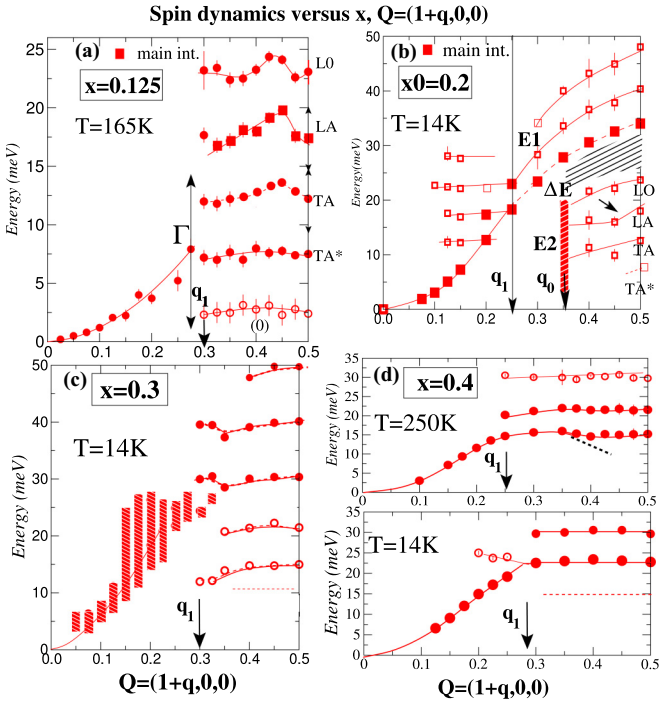

FIG. 1. Spin dynamics spectra of $La_{1-x}Sr_xMnO_3$, along Mn-O-Mn. The q_1 value indicates the limit of the discrete energy spectrum. At $x_0 = 0.2$ two q limits appear, defined by $q_0 \approx 0.35$ r.l.u. and $q_1 \approx 0.25$ r.l.u. At $x = 0.125$ and $x_0 = 0.2$, the square symbols correspond to the excitations with main intensity. The continuous lines are guides for the eye. The pattern styles are unresolved excitations. (a) $x = 1/8$, $T = 165$ K. The empty circles of the lowest energy level (○) are temperature dependent (see text). Γ shows the full energy width at half maximum (b) $x_0 = 0.2$, $T = 14$ K. The hatched area indicates an energy separation between the E_1 and E_2 ranges. (c) $x = 0.3$, $T = 14$ K. (d) $x = 0.4$, $T = 14$ K (lower) and $T = 250$ K (upper). The black dotted line shows the tendency for Brillouin zone folding.

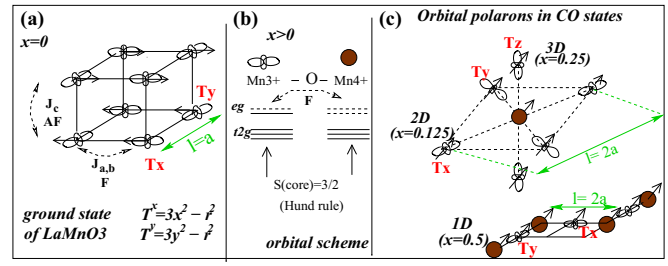

FIG. 2. (a) Staggered pattern of the orbital states T_x and T_y in the (a, b) planes of the pseudocubic $LaMnO_3$. It determines a spin coupling F in (a, b) planes and AF along c according to the Goodenough-Kanamori rules. (b) Scheme of the orbital states of the Mn^{3+} and the Mn^{4+} ions. (c) Evolution with x of the shape or the dimension D of the orbital polarons taken in Ref. [6] in the charge-ordered (CO) states of manganites.

Our present analysis is based on the two following observations. First, as shown in Fig. 1, the $E_n^{\rm mag}(q)$ spectrum appears in a well-defined q range above the specific value q_1 indicated by the arrows in Fig. 1. Below q_1, the spin excitation spectrum is essentially represented by the quadratic spin-wave dispersion law $E \sim \mathcal{D}q^2$, with the stiffness constant $\mathcal{D}$, typical of the ferromagnetic metallic state at $T \leqslant T_c$. This defines a wave-vector scale which separates "collective" or "global" magnetic excitations for $q \leqslant q_1$ from "individual" or "local" ones for $q \geqslant q_1$. In the intermediate $q_1/2 \leqslant q \leqslant q_1$ range, the two types of excitations coexist. This is especially well observed for $x_0 = 0.2$ and $x = 0.3$.

Next, we follow the idea that the discrete magnetic spectrum $E_n^{\rm mag}(q)$ results from the existence of "orbital polarons" in a (quasi)metallic state. Such a polaron has been introduced in manganites because of the anisotropic shape of the d orbital. It consists of a cluster of neighboring Mn^{3+} sites whose d orbitals point toward a central Mn^{4+} hole, hence optimizing covalency effects [6]. In charge-ordered states, the polaron is ferromagnetic (F), as shown in Fig. 2(c). To describe this picture, we recall that each Mn^{3+} ion hosts four electrons [see the scheme in Fig. 2(b)]. Three of them are in a t_{2g} orbital state and, because of Hund's rule, form an electrically inert core spin $S = 3/2$. The outer one is in a Jahn-Teller active orbital state corresponding to either the $x^2 - y^2$ type (T_z) or $3x^2 - r^2$ (T_x), $3y^2 - r^2$ (T_y), and $3z^2 - r^2$ (T_z) states, with a spin $S = 1/2$ also aligned with the core spin. In the parent orthorhombic $LaMnO_3$, a cooperative Jahn-Teller effect lifts the orbital degeneracy by forming a staggered pattern of T_x and T_y components, from which the magnetic structure of ferromagnetic (a, b) planes stacked antiferromagnetically along c is obtained via the Goodenough-Kanamori rules [Fig. 2(a)]. The $E_n^{\rm mag}(q)$ spectrum appears upon doping, as the antiferromagnetic (AF) exchange $J_c(x)$ vanishes and the quasimetallic state arises. There, as the hole at the center Mn^{4+} of the polarons is hopping, the orbitals of the Mn^{3+} neighbors fluctuate to accommodate its new position. Equivalently, the hole mixes dynamically all the possible orbital configurations of its Mn^{3+} neighbors with degenerate energies [32]. In these compounds where the orbital-phonon coupling is expected to be strong [33], the phonons lift the orbital quantum degeneracy through a dynamical Jahn-Teller effect. Some constraints on the hole hopping [34] and on the orbital structure of the polarons suggest that the T_x, T_y, and T_z orbital states are mainly concerned with this mixing. In the case where all sites are Mn^{3+} ions, the interplay between the spin and orbital operators arises from the crossed term $\sum_{i,j}(S_iS_j)(T_iT_j)$ of the Kugel-Khomskii Hamiltonian [35]. In a mean-field approach, the product of operators can be uncoupled and averaged to $\langle S_iS_j\rangle T_iT_j$ [36]. These spin-orbital excitations appear as orbital excitations with an intensity proportional to the squared magnetization $\langle S_iS_j\rangle \propto M^2(T)$. Experimentally, two situations occur. In the metallic state ($x = 0.3$ and $x = 0.4$ at $T = 14$ K) the excitations are independent of wave vector and temperature and their relative intensity agrees with the squared magnetization $M^2(T)$. In this limit, which corresponds to an "orbital liquid state" [32], the magnetization arises from the collective or global spin-coupling effect. In contrast, at lower doping ($x = 0.125$ and $x = 0.2$) and at larger doping close to $x = 0.5$ (our data taken with $x = 0.4$ at $T = 250$ K), the energy levels exhibit a q dispersion and a temperature dependence. A local spin coupling is superimposed over the effect of orbital fluctuations, which reveals the existence of correlations between the orbital polarons.

The splitting of the orbital degeneracy by phonons allows one to determine the number of orbital degenerate states n. It

corresponds to the number of possible orientations of the orbital states involved in the orbital polarons. It therefore varies with the dimension D of the orbital polarons. Its evolution with x has been shown in the case of the charge-ordered states [6] and is illustrated in Fig. 2(c). At small x values ($x \leqslant 0.2$), the orbital polaron is essentially a "2D" object with four Mn^{3+} sites surrounding a central Mn^{4+} ion, as a consequence of the 2D orbital ordering observed at $x = 0$. At larger doping ($x = 0.25$), it becomes "3D" with six Mn^{3+} sites surrounding a central Mn^{4+} ion. It shrinks beyond this doping value because of steric hindrance so that, at $x = 0.5$, specific zigzag paths of orbitals set in with two Mn^{3+} sites surrounding a central Mn^{4+} site. In this charge-ordered structure (CE) the zigzag chains are ferromagnetic with an AF interchain coupling [37]. Experimentally, at $x = 0.125$ (2D), $n = 4$. As argued below, the lowest energy level being temperature dependent, should not be numbered. It may correspond to the (x, x), (x, y), (y, x), and (y, y) fluctuations of orbital orientations. The number increases to $n \approx 8$ at $x = 0.3$ in the 3D metallic state where nine possibilities are expected for the fluctuations between the x, y, and z orbital orientations, and decreases to $n = 2 \approx 3$ at $x = 0.4$ in agreement with the expected evolution.

In this direct space picture, the characteristic q scale of the excitations defined by q_1 can be transformed back to real space to get the size of the polaron via the relation $\ell = 0.5a/q_1$. Here, the minimum q-scale value ($q_1 = 0.5$) is related to the lattice spacing a. This relation is valid as long as the excitations are localized (or q independent) and originate from a coupling with the lattice (here with the phonons). This relation tells us that for $q_1 \approx 0.25$ reduced lattice units (r.l.u.), the size of the cluster along Mn-O-Mn directions is close to two lattice spacings.

Within this analysis, the spin dynamics reveals the existence of orbital polarons which evolve with x into three steps $x \leqslant x_0$, $x \approx x_0$, and $x \geqslant x_0$. For $x \neq x_0$ only one q scale is observed which defines a size of polaron close to $2a$ either coupled ($x = 0.125$) or uncoupled ($x = 0.3$). For $x \approx x_0$, two q scales are observed, both in the spin and the lattice dynamics, and characteristics of a local "ground state." The latter is defined by both the commensurate size of polarons ($2a$) defining chains, and by their periodic distribution ($\lambda \approx 3a$).

The paper is organized as follows. Section II A describes the spin dynamic spectrum within the new analysis at $x = 0.125$ and $T_{o'o''} \leqslant T \leqslant T_c$. Section II B, devoted to $x_0 = 0.2$, presents both the spin dynamics spectrum within the new analysis for $T \leqslant T_c$ in (1), and the lattice excitations in the acoustic range for $T \geqslant T_c$ and $T \leqslant T_c$ in (2). Section II C describes the spin spectrum within the new analysis in the metallic state, at $x = 0.3$ and $x = 0.4$ ($T \leqslant T_c$). Section III provides the discussion and conclusion.

Inelastic neutron scattering experiments were carried out at the Laboratoire Leon Brillouin using cold and thermal neutron three-axis spectrometers (TAS) 4F1, 1T, and 2T and at the Institut Laue Langevin using thermal neutron TAS IN8. The instrument configuration and resolution was in each case adapted to the studied momentum and energy range. The crystal structure of the studied phases is either weakly orthorhombic ($x = 0.125$, $x_0 = 0.2$) or rhombohedral ($x = 0.3$, 0.4) with a rhombohedral to orthorhombic transition at $T = 170$ K at $x = 0.175$ [31]. It is averaged for simplicity to a pseudocubic structure with $a \approx 3.9$ Å. Only the Mn-O-Mn bond direction or [100] symmetry direction is considered here. The wave vector q is expressed in reduced lattice units r.l.u. (in units of $2\pi/a$) along the symmetry direction [100]. The magnon measurements have been performed at $Q = q + \tau$ with $\tau = (1, 0, 0)$. At $x_0 = 0.2$, the phonons are distinguished from magnons by changing the Brillouin zone τ in the total wave vector Q where $Q = q + \tau$ and by using the effect of temperature ($T \geqslant T_c$).

II. EXPERIMENTS

A. The quasimetallic regime, $x = 0.125$, $T \geqslant T_{o'o''} = 159$ K, $T_c = 181$ K

The spin dynamics spectrum reported in Fig. 1(a) has been measured in the whole q range at $T = 165$ K ($T_{o'o''} \leqslant T \leqslant T_c$), and at one q value ($q = 0.5$ r.l.u.) as a function of temperature up to 250 K along Mn-O-Mn and up to 292 K in other symmetry directions. In the small-q range, the stiffness constant $\mathcal{D}$ (global coupling) has a 2D character [26]. The acoustic phonon excitations have been also measured but not reported here. An example of raw data is shown at $q = 0.15$ r.l.u. in Fig. 3(a). The fast increasing damping Γ of the excitations which follows a $\Gamma = Aq^{2.5}$ law at $T = 165$ K smears the transition between the small-q and the large-q regimes [inset in Fig. 3(b)]. As shown from the raw data previously reported for four q values [26], the $E_n^{\text{mag}}(q)$ spectrum consists of four equidistant levels separated by $\approx$5 meV, namely, 22.5, 17, 12, and 7.5 meV at $q = 0.5$ r.l.u. The lowest energy level, $E(0) \approx 2.5$ meV, is not considered. It is actually temperature dependent since it disappears in the "charge-ordered" state ($T \leqslant T_{o'o''}$) in contrast with the four q-dispersed energy levels which are in coincidence with the q-dispersed phonons [28]. It therefore looks like an anisotropy gap of magnetic and possibly structural origin and should not be considered when numbering the energy levels related to orbital degeneracy.

The energy $E_n^{\text{mag}}(q)$ values observed at $q = 0.5$ r.l.u. correspond successively to the $q = 0.5$ r.l.u. phonon excitations LO, LA, and TA reported in Fig. 4 for $x_0 = 0.2$. The value $E \approx 7.5$ meV is related to a TA* branch, specific for $x = 0.125$. From the $q_1 = 0.3$ r.l.u., a "size" of polarons $\ell \approx 1.7a$ ($\ell = 0.5a/q_1$) is deduced along the Mn-O-Mn bond directions, indicating a strong lattice contraction. The most surprising observation here is the existence of a q dispersion with a maximum of energy at $q = 0.45$ r.l.u. This is particularly clearly observed for the energy level $E \approx 17$ meV with strongest intensity. Such a q dependence may be interpreted as an AF coupling between two neighbor F polarons, each of them being on a contracted lattice scale $\ell \approx 1.7a$. It corresponds to the pairing of two polarons (or bipolarons) in a singlet state. Actually the incommensurability provides a complexity to the analysis which leads us to explain this observation in a further work. The discrete spectrum is still observed at 250 K, well above T_c (181 K) superimposed on a quasielastic signal, typical of a paramagnetic state. Corresponding raw data are reported in Fig. 3(c). It is no longer observed at 292 K in agreement with NMR experiments [38]. This is illustrated in the inset of Fig. 3(c′) along the symmetry direction [111].

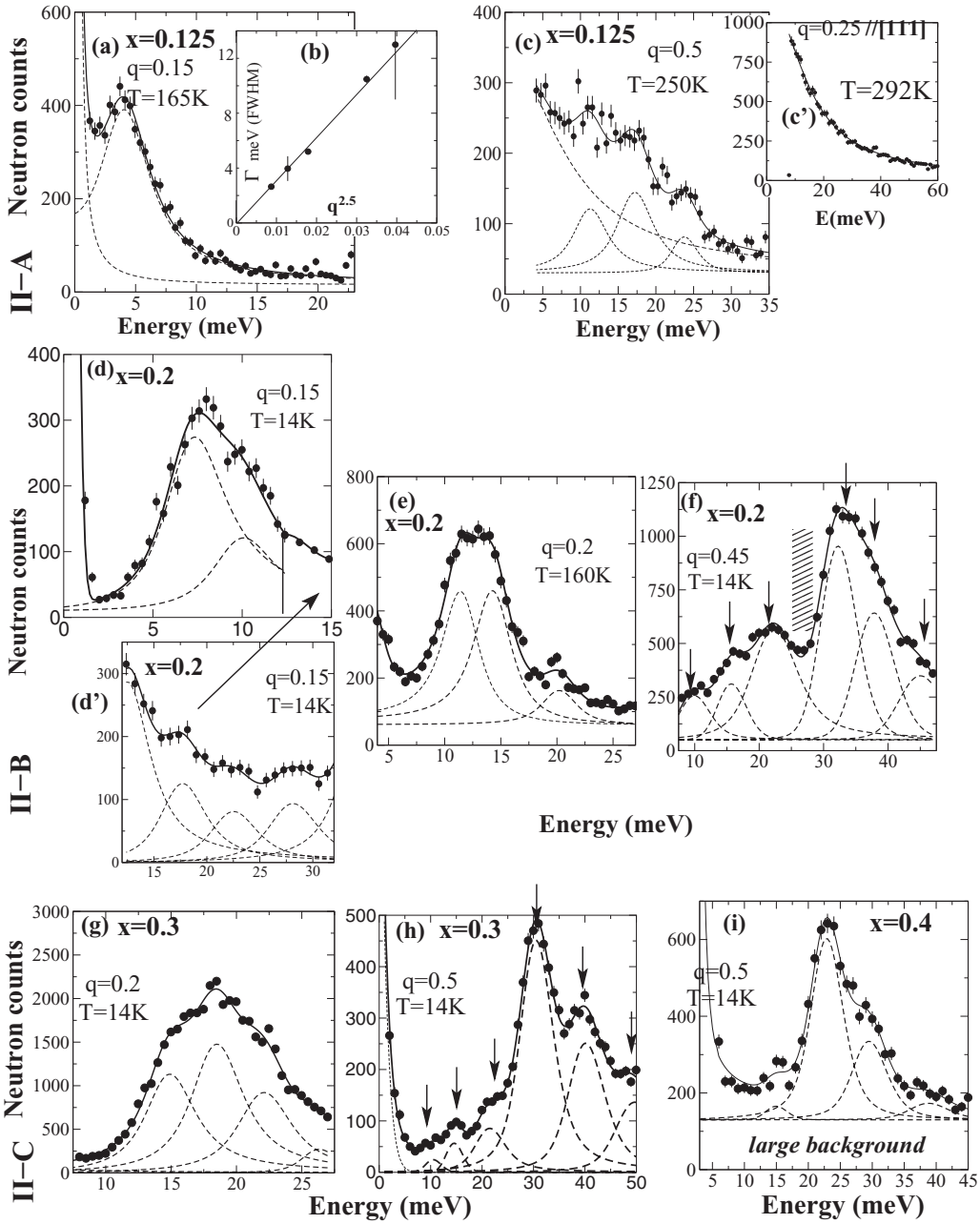

FIG. 3. Raw data corresponding to the spin dynamic spectra $E(q)$ in the three regimes II-A, II-B, and II-C at small $q \leqslant q_1$ and large $q \geqslant q_1$ q values. The wave vector q is expressed in reduced lattice units (r.l.u.). The data are fit by Lorentzian line shapes to account for damping, convoluted with the resolution function of the three-axis spectrometers. In the large-q range, the intrinsic energy linewidth (full width at half maximum) is $\Gamma \approx 4$–6 meV. II-A: $x = 0.125$. (a) $q = 0.15$, $T = 165$ K ($T_{o'o} \leqslant T \leqslant T_c$). (b) Inset: $q^{2.5}$ dependence of the energy linewidth Γ. (c) $q = 0.5$, $T = 250$ K ($T \geqslant T_c$). (c′) Inset: $q = 0.25$, $T = 292$ K along [111]. II-B: $x_0 = 0.2$. (d) $q = 0.15$, $T = 15$ K with the tail of energy modulations in (d′),(e) $q = 0.2$, $T = 160$ K for a direct comparison with $x = 0.125$. (f) $q = 0.45$, $T = 15$ K. The pattern style corresponds to ΔE (see the text). II-C: (g) $x = 0.3$, $q = 0.2$, $T = 14$ K. (h) $x = 0.3$, $q = 0.5$, $T = 14$ K. The temperature-dependent spectra have been reported in Ref. [27]. (i) $x = 0.4$, $T = 15$ K.

B. The transitory regime: $x = 0.2$, $T_c = 301$ K with optimal magnetoresistance

1. The spin dynamics spectrum

In Fig. 1(b) at $T = 14$ K the spin dynamics spectrum exhibits a change in energy scale by a factor 2 with respect to that observed at $x = 0.125$. Raw data are reported in Figs. 3(d), 3(d′), 3(e), and 3(f). In the large-q range, at $q =$ 0.35 r.l.u., an interval $\approx$8 meV appears which is larger by $\Delta E \approx 3$ meV than the interval $\approx$5 meV of the lower energy range. It is indicated by the hatched area in Fig. 1(b) and in Fig. 3(f). This $\Delta E(q = 0.35 \text{ r.l.u.}) = 3$ meV separates two zones of discrete spectrum E_2 ($\leqslant$25 meV) and E_1 ($\geqslant$25 meV) with two typical q dependences. E_2 with four energy levels in the same energy range as $x = 0.125$, corresponds to the "in-plane" or (x, y) orbital fluctuations, so that E_1, at higher

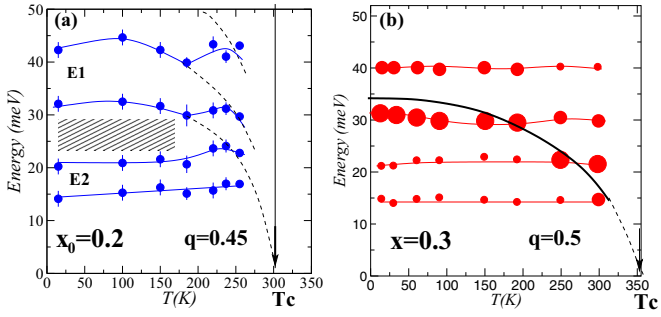

FIG. 4. Temperature evolution of the four central energies of the $E_n^{\mathrm{mag}}(q)$ spectrum (a) at $x_0 = 0.2$ for $q = 0.45$ r.l.u. and in (b) at $x = 0.3$ for $q = 0.5$ r.l.u. The dashed and continuous lines are guides for the eyes. In (a) the black pattern indicates the separation in energy scale: between the low-energy excitations, temperature independent, with energy values equal to the phonon energies measured at $q = 0.5$ r.l.u. reported in Fig. 5, and the high-energy ones, temperature dependent, which follow variation of $\mathcal{D}(T)$. In (b), the distribution of the intensity over the dynamic spin spectrum is shown by circles of varying size. The black line indicates the variation of the energy with the strongest intensity as a function of temperature while approaching T_c.

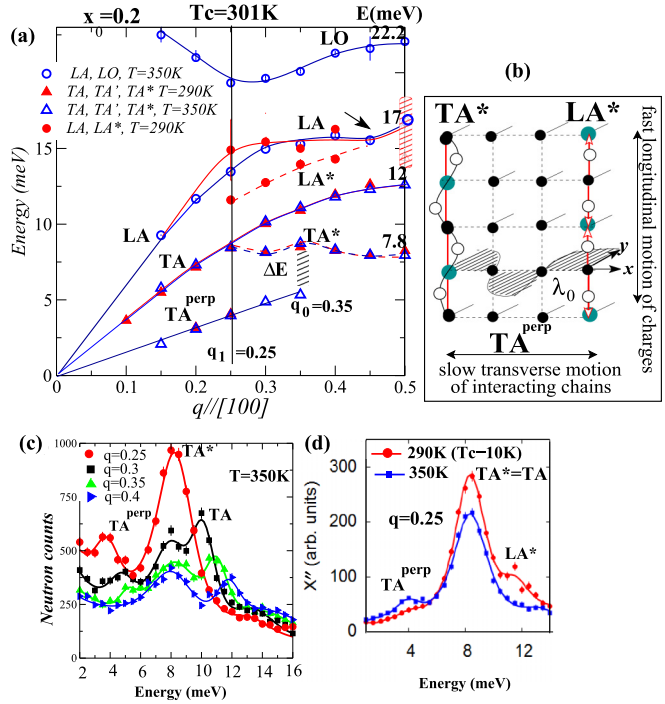

FIG. 5. (a) Lattice dynamics spectrum ($E \leqslant 25$ meV) for $T = 350$ K (filled symbols) and $T = 290$ K (open symbols) measured at $x = 0.2$. The LA branch evolves at $T \leqslant T_c$ indicating a repulsive effect with the new LA* branch which occurs in the [0.25–0.5] q range. The red pattern style at $q = 0.5$, $E \sim 15$ meV indicates a broadening induced by the interaction between the LA and LA* excitations. The arrow in the LA branch indicates an anomaly in energy also observed in the quantized spin spectrum of Fig. 1(b). The black pattern style defines the interaction energy $\Delta E = 3$ meV at $q_0 = 0.35$ r.l.u. between the TA* and $\mathrm{TA}^{\mathrm{perp}}(q)$ branches. (b) Instantaneous picture of interacting chains of ordered "orbital polarons" of size $2a$ in one of the (x, z) planes. Chains are stretched along the z direction and separated by $\approx 3a$ in the x direction. Planes are supposed not to be correlated in the y direction. The blue circles correspond to Mn^{4+}, the black ones to Mn^{3+}, and the empty ones to O atoms. The TA* and LA* branches correspond to acoustic excitations with, respectively, a transverse and stationary character or a longitudinal and propagating one with wave vector along the chains. The $\mathrm{TA}^{\mathrm{perp}}(q)$ branch corresponds to slower and propagating transverse fluctuations of at least two interacting chains with a distance between them defined by $q_0 \leqslant 0.35$ r.l.u. or $\lambda \geqslant \lambda_0 = 2\pi/q_0 \approx 3a$. (c) Raw data corresponding to the transverse acoustic phonons as a function of q for $T \geqslant T_c$, showing the disappearance of $\mathrm{TA}^{\mathrm{perp}}(q)$ at $q = 0.4$ r.l.u. (d) Raw data corresponding to $q = 0.25$ at $T = 350$ K $\geqslant T_c$ and $T = 290$ K $\leqslant T_c$ corrected by the detailed balance factor.

energy, is attributed to new "out-of-plane" ones. The energy ΔE between the two zones E_1 and E_2 indicates the existence of a connection between the in-plane and the out-of-plane orbital fluctuations. At $T = 14$ K, the zone $E_2(q)$ appears at $q_0 \geqslant 0.35$ r.l.u. where the discrete levels follow the q-dependent phonon branches. This can be in particular verified for LA(q) where the anomaly in the q dispersion indicated by an arrow at $q = 0.45$ r.l.u. in Fig. 1(b) is also observed in the LA*(q) branch reported below in Fig. 5(a). We remark that such a feature was observed for the q-dependent magnon-phonon coincidence at $x = 1/8$, $T \leqslant T_{o'o''}$ (Ref. [28]). It indicates the existence of strong orbital correlations along the Mn-O-Mn bond directions in the plane, the consequence of a charge ordering with a cut-off value $q_0 \approx 0.35$ r.l.u. This value determines a periodic distribution of charges with period $\lambda_0 = 2\pi/q_0 \approx 3a$.

The higher energy $E_1(q)$ zone may be analyzed as the superimposition of two spectra of distinct origins. One, q independent, spreading on the [0.25–0.5] q range, determines links of $2a$ size along the z direction perpendicular to the (x, y) planes. The other one, q dependent, defines a cosine law which approximately fits to the $\mathcal{D}q^2$ law defined in the small-q range. This q dependence is actually observed in the whole temperature range $T \leqslant T_c$. This is shown in Fig. 4(a) where a T-dependent variation can be drawn through the energy values, corresponding to $\mathcal{D}(T)$ (stiffness constant) or to the squared magnetization $M^2(T)$. Therefore, the magnetic excitations of the large-q range related to the orbital correlations along z exhibit a collective character which arises from the same ferromagnetic state as the magnetic excitations of the small q range. Finally, a quantized spectrum with a weak intensity is also observed in the q range of the "collective" excitations above the quadratic $\mathcal{D}q^2$ down to $q = 0.125$ r.l.u. [Fig. 1(b)] with raw data in Figs. 3(d′) and 3(e). It defines a $4a$ scale as for two orbital polarons of $2a$ size in contact one to the other. No further scale can be observed which is consistent with the situation in metals where, as q goes to zero, a sum rule of intensity exists in favor of the Goldstone mode $(q = 0, E = 0)$ of the collective excitations.

From these observations, a picture of phase separation into ferromagnetic chains arises. The chains consist of orbital polarons of $2a$ size with a periodic distribution $\approx 3a$ in the perpendicular bond direction of the plane which contains the chains. This description corresponds to a 2D picture which, if long range, would lead to $x = 1/6 \approx 0.17$, close to the x value

for optimal doping [31]. The tendency for ordered orbitals to define planes is well known [32]. In 3D space we may assume the existence of several equivalent planes fluctuating in time, with a weak interaction between them. This picture of interacting chains is supported by the interaction with the lattice described below.

2. The lattice dynamics spectrum

Figure 5(a) displays low-energy ($E \leqslant 25$ meV) phonon excitations with longitudinal and transverse character obtained at $T = 350$ K ($T \geqslant T_c$) and $T = 290$ K, $T \leqslant T_c$) along Mn-O-Mn. Corresponding raw data are displayed in Figs. 5(c) and 5(d). The transverse and the longitudinal excitations have been obtained by using distinct experimental configurations. Here, the scattering of magnetic origin is a background in the raw data with intensity reduced by the form factor of Mn ions. At $T = 350$ K, a nearly constant-energy value, $E \approx 8$ meV, is observed in the [0.25–0.5] q range, labeled TA*. It is connected with the TA(q) branch of the 3D pseudocubic structure at $q_1 = 0.25$ r.l.u. At lower energies, a dispersed TA$^{\rm perp}(q)$ branch is observed up to $q_0 = 0.35$ r.l.u., where a small shift in energy appears in TA*, defining $\Delta E(q_0 = 0.35$ r.l.u.$) = 3$ meV. At $T = 290$ K, $\leqslant T_c$, the TA$^{\rm perp}(q)$ branch has nearly disappeared. In contrast, the TA* one persists with the same behavior at $q_0 = 0.35$ r.l.u. and with an increasing intensity at the $q = 0.25$ r.l.u. value. Such an increase is in contradiction with the Bose factor, similarly to previous observations reported at higher energy [11,12]. Concomitantly, new excitations occur in the [0.25–0.5] q range, such as the dispersed LA* branch just below the usual LA(q) branch which consequently is shifted to higher energy values, especially close to $q = 0.25$ r.l.u. These observations are analyzed as follows.

The existence of two transverse acoustic branches, TA* and TA$^{\rm perp}(q)$, reveals a privileged direction among the three Mn-O-Mn bond directions, induced by the charge-phonon coupling, so that the transverse acoustic excitations with wave vectors q parallel to that direction (TA*) are distinct from those with wave vectors q perpendicular to it [TA$^{\rm perp}(q)$]. An instantaneous picture of two chains with transverse excitations, TA* and TA$^{\rm perp}(q)$, is shown in Fig. 5(b). Moreover, the TA* and TA$^{\rm perp}(q)$ branches are defined in two separate energy ranges so that they are characteristic of two distinct time scales of lattice vibrations. The propagating TA$^{\rm perp}(q)$ branch, at low energy, corresponds to slow transverse fluctuations of interacting chains within a plane. During this slow fluctuation time, faster excitations occur with q parallel to the direction of the chains, either transverse and stationary corresponding to the TA* branch, or longitudinal and propagating corresponding to the LA* branch. Both types of excitations are observed in the [0.25–0.5] q range, which is characteristic of the $2a$ scale expected for orbital polarons in contact each with the other. The lock-in of the TA* branch at $q = 0.25$ r.l.u., ensures the structural and electrical stability of this charge-orbital-lattice-ordered structure whatever the directions of the interacting chains in 3D space. These features are observed even at $T = 350$ K above T_c (301 K). The interaction energy $\Delta E = 3$ meV between TA$^{\rm perp}$ and TA* occurs at $q = 0.35$ r.l.u. This q value determines the same periodic distribution of the chains in the planes as that observed in the magnetic discrete spectrum described above. The difference, however, is that this periodic distribution is defined here in the complementary q range ($q_x, q_y \leqslant 0.35$ r.l.u.), by a maximal instead of a minimal wave-vector limit q_0. We can conclude that this local charge-ordered structure is stabilized by a delicate equilibrium between all the degrees of freedom. The occurrence of an increasing intensity of TA* at the $q = 0.25$ r.l.u. value for $T \leqslant T_c$, indicates a phase coherence between the localized TA* acoustic excitations. It appears at $T \leqslant T_c$ concomitantly with the propagating LA*(q) excitation and is therefore induced by the cooperative motion of the charge carriers along the chains. Coming back to the spin dynamic spectrum, we see here evidence that the enhancement of the ferromagnetism is induced by the cooperative mobility of the charge carriers along the chains. The TA$^{\rm perp}(q)$ branches are observable as long as its own characteristic time, $1/f$, deduced from its frequency values f, is faster than the lifetime of the chains, which actually decreases as the temperature is lowered. As shown at $T = 290$ K in Fig. 5(d), the acoustic transverse fluctuations TA$^{\rm perp}(q)$ progressively disappear below T_c.

C. The metallic regime
$x = 0.3$ ($T_c = 358$ K), $x = 0.4$ ($T_c = 315$ K)

At $x = 0.3$, $T_c = 358$ K, the spectrum reported in Fig. 1(c) at $T = 14$ K with raw data in Fig. 3(h) extends on the [$\approx$0.3–0.5] q range. It indicates a lattice contraction ($\ell \approx 1.7a \leqslant 2a$) for the "size" of the orbital polarons in all bond directions, similar to that observed in the quasimetallic state ($x = 0.125$). The energy levels are nearly q independent in the [0.3–0.5] q scale but also temperature independent, as seen in Fig. 4(b). The corresponding raw data have been reported in Ref. [27]. The energy values $E = 15$ meV and $E = 21$ meV of the $E_n^{\rm mag}$ spectrum ($E \leqslant 25$ meV), slightly smaller than those observed at $x = 0.125$, agree with the q average of the phonon energies on the q range of the polarons. This tight relation with phonon states reveals an absence of direct or local spin coupling, indicating an "orbital liquid" state [32]. The magnetic character of the excitations appears in the distribution of intensity among the discrete $E_n^{\rm mag}$ values. Although the energy values are temperature independent, their relative intensity is temperature dependent. By using the raw spectra observed at $q = 0.5$ r.l.u. reported in the Fig. 4 of Ref. [27], the energy with maximal intensity can be reported at each temperature. It provides the black line of Fig. 4(b).

At the nominal $x = 0.4$ doping value, the observed $E_n^{\rm mag}$ spectrum displayed in Fig. 1(d) with raw data in Fig. 3(i) exhibits the same energy values as those observed at $x = 0.3$ with a decrease of the n value ($\approx$2 or 3 at $T = 14$ K). This evolution occurs with a decrease of the stiffness constant $\mathcal{D}$ at $T = 14$ K and of the T_c values with respect to $x = 0.3$. In the upper panel of Fig. 1(d) the discrete spectrum determined at $T = 250$ K spreads on the [0.25–0.5] q scale and exhibits a tendency for folding the Brillouin zone outlined by a dotted black line. This is the consequence of the slowing down of the orbital fluctuations upon approaching T_c, as expected for a doping value close to $x = 0.5$. Due to the steric hindrance, the orbital fluctuations should occur along 1D paths defined

by the hopping holes with T_x, T_y, and T_z orbital states, close to the zigzag paths of orbitals proposed in the charge-ordered state $x = 0.5$ [6] and illustrated in Fig. 2(d). This analysis is very close to that used to interpret the spin dynamics of the narrow electronic band $Sm_{0.55}Sr_{0.45}MnO_3$ in the $x = 0.5$ limit [21].

III. DISCUSSION AND CONCLUSION

The main results of our analysis are summarized as follows. In the low and large doping range where $q_1 = 0.3$ r.l.u. the spin spectrum reveals orbital polarons with the size $\ell \approx 1.7a$ along the Mn-O-Mn bonds which is characteristic of a strong lattice contraction. They appear either with a 2D character and F polarons paired by an AF coupling ($x = 0.125$ in quasimetallic state) or with a 3D character and "free" from any direct or local spin coupling ($x = 0.3$ and $x = 0.4$ in the metallic state $T = 14$ K). At the intermediate $x_0 = 0.2$ value, the spin spectrum is richer. It reveals two q ranges, [0.35–0.5] and [0.25–0.5] associated with two distinct energy ranges corresponding to in-plane and out-of-plane correlated orbital fluctuations, separated by the energy $\Delta E = 3$ meV. The same q ranges are observed in the transverse acoustic excitations of the lattice with a q wave vector respectively along one bond and perpendicular to it. Both types of excitations reveal the existence of chains consisting of orbital polarons of size $2a$, with a periodic distribution $3a$ in the plane of the chains. At $T \leqslant T_c$, the charges propagate together with the longitudinal acoustic phonons along the chains, enhancing their ferromagnetic character. This picture corresponds to a phase separation. The magnetic signature of this phase separation appears in the q dispersion of the spin dynamics when considering the excitations with principal intensity [square symbols in Fig. 1(b)]. There, the q dispersion is very close to a cosine law and therefore can be nearly fitted by using one phenomenological constant J_1 between the first neigbor spins. In that analysis, at $x \approx x_0$, the small-q ($q \leqslant 0.25$ r.l.u.) and large-q ($q \geqslant 0.25$ r.l.u.) ranges of the magnetic excitations are the collective excitations of the same ferromagnetic state. This contrasts with the $x \neq x_0$ case where the large-q excitations give rise to a hardening ($x \leqslant x_0$) or a softening ($x \geqslant x_0$) (Fig. 1) so that additional phenomenological constants are required to fit the whole range of excitations. In these ferromagnetic chains, the magnetic and the conduction properties are coupled together. This may appear in the fact that the $q_0 = 0.35$ r.l.u. wave-vector value which determines the periodic distribution of the chain $\lambda \approx 3a$ appears as a minimum or a maximum wave-vector value of the excitations depending on their magnetic or lattice origin. We conclude that these observations characterize a phase separation between metallic and ferromagnetic chains embedded in a nonmetallic matrix.

Owing to the CMR effect, a magnetic field applied at T_c would interact with the magnetic chains and, by the way, would enhance the conduction of orbital polarons along the chains with spin-charge-orbital and structural degrees of freedom coupled together. The small magnitude of the interaction energy between the chains, $\Delta E \approx 3$ meV, which stabilizes this local ground state, agrees with predictions [1]. This nematiclike picture was actually also predicted for cuprates [39]. In theoretical works, the large magnetoresistance has been first related to a crossover between a strong and a weak regime for the J/W ratio and qualitatively interpreted in a Kondo lattice model [40]. It was then shown that the double exchange mechanism introduced by Zener [41] could not explain quantitatively the effect of CMR, and that the charge-lattice coupling would be necessary [42]. The present picture conciliates these two effects. The bipolaron-polaron transition predicted at T_c is not observed [43].

Many experiments have been also performed in compounds with a narrow electronic bandwidth such as $La_{1-x}Ca_xMnO_3$. Here, at least in the metallic state, the magnetic excitations cannot be resolved into distinct energy levels. We recall that it is thanks to the observation of several energy levels and of their relation with phonon energies that the role of the orbital fluctuations in the magnetic excitations has been evidenced in the present work. In spite of differences between compounds with large and narrow electronic bands indicated by smaller T_c values and by distinct lifetimes for the CE correlated polarons observed at $T \geqslant T_c$ [17], we suggest that a similar effect could exist as a function of doping x.

In the narrow band $La_{1-x}Ca_xMnO_3$ the optimum of CMR is expected to occur at $x(\mathrm{Ca}) = 1/3$. In the quasimetallic state corresponding to the $x(\mathrm{Ca}) = 0.17$ and $x(\mathrm{Ca}) = 0.2$ doping values, a previous determination of the spin spectrum has revealed the existence of four discrete energy levels in the [0.3–0.5] q range and $E \leqslant 22.5$ meV [44]. We remark that these observations are close to those reported at $x(\mathrm{Sr}) = 0.125$, which characterize 2D orbital polarons. At larger $x(\mathrm{Ca})$ values, the discreteness of the spectrum is smeared out so that the role of the phonons cannot be observed. In a first experiment with the nominal concentration $x(\mathrm{Ca}) = 0.3$, a broad magnetic excitation spectrum was reported at $E \approx 22.5$ meV in the large q range [0.3–0.5] resulting into a flattening when considering the whole q dispersion [20]. This behavior corresponds to the observations reported here at $x(\mathrm{Sr}) = 0.3$. Later, two other experiments have determined the spin dynamics at the same nominal $x(\mathrm{Ca}) = 0.3$ doping value but with a larger T_c value [23,24]. The softening effect of the energies at the zone boundary was found to be null [23] or small [24] so that the whole q dispersion can be described mainly by one phenomenological ferromagnetic J_1 coupling constant. These observations recall those reported here at $x_0(\mathrm{Sr}) = 0.2$. In the most recent study, an increase of the damping of the excitations was observed along Mn-O-Mn bonds at $E \geqslant 15$ meV or $q \geqslant 0.25$ r.l.u., interpreted as the effect of a phase separation picture [24]. Experiments by transmission electronic microscopy have indicated the existence of small charge-ordered domains with, however, a too small size to be characterized [45]. These considerations may suggest the existence of a local charge-ordered state at the doping value with maximum magnetoresistance.

In summary, our study provides evidence for a spin dynamics characterized by discrete magnetic energy spectra $E_n^{\mathrm{mag}}(q)$ and their direct relation with lattice dynamics in the acoustic range at $x_0 = 0.2$. The $E_n^{\mathrm{mag}}(q)$ spectrum is understood as arising from the internal excitations of orbital polarons, which can be seen as a hole (Mn^{4+}) interacting with orbitals of the nearest adjacent Mn^{3+} ions. The hopping mixes dynamically

all the possible orbital configurations of those surrounding Mn^{3+} whose degeneracy is lifted by low-energy phonons. Furthermore, the shape of those polarons evolves with doping. At the transition between their 2D and 3D evolution, interacting chains of polarons form and longitudinal acoustic excitations reveal the propagation of these polarons along the chains at $T \leqslant T_c$. This phase separation between metallic and ferromagnetic chains in a nonmetallic matrix, may be crucial for CMR.

ACKNOWLEDGMENTS

An important part of this experimental work has been done with F. Moussa and B. Hennion. They are gratefully acknowledged. The authors are also very indebted to S. Aubry, Y. Sidis, F. Onufrieva, and J. W. Lynn for many fruitful discussions. The work at the Peter the Great St. Petersburg Polytechnic University was supported by the Ministry of Education and Science of Russian Federation (Grant No. 3.1150.2017/4.6).

[1] E. Dagotto, Science **309**, 257 (2005).
[2] H. Ulbrich and M. Braden, Physica C **481**, 31 (2012).
[3] S. Anissimova, D. Parshall, D. Lamago, G. D. Gu, M. D. Lumsden, Songxue Chi, J. A. Fernandez-Baca, D. L. Albernathy, J. M. Tranquada, and D. Reznik, Nat. Commun. **5**, 3467 (2014).
[4] J. Tao, K. Sun, W.-K. Yin, H. Xin, J. G. Wen, W. Luo, S. J. Pennycock, J. M. Tranquada, and Y. Zhu, Sci. Rep. **6**, 37624 (2016).
[5] Mengkun Liu, Aaron J. Sternbach, and D. N. Basov, Rep. Prog. Phys. **80**, 014501 (2017).
[6] T. Mizokawa, D. I. Khomskii, and G. A. Sawatzky, Phys. Rev. B **61**, R3776 (2000); **63**, 024403 (2000).
[7] J. W. Lynn, R. W. Erwin, J. A. Borchers, Q. Huang, A. Santoro, J.-L. Peng, and Z. Y. Li, Phys. Rev. Lett. **76**, 4046 (1996).
[8] J. M. de Teresa, M. R. Ibarra, P. A. Algabarel C. Ritter, C. Marquina, J. Blasco, J. Garcia, A. del Moral, and Z. Arnold, Nature (London) **386**, 256 (1997).
[9] J. W. Lynn, J. Supercond. **13**, 263 (2000).
[10] W. Reichardt and M. Braden, Physica B **263-264**, 41 (1999).
[11] J. Zhang, P. Dai, J. A. Fernandez-Baca, E. W. Plummer, Y. Tomioka, and Y. Tokura, Phys. Rev. Lett. **86**, 3823 (2001).
[12] F. Weber, D. N. Argyriou, O. Prokhnenko, and D. Reznik, Phys. Rev. B **88**, 241106(R) (2013).
[13] C. P. Adams, J. W. Lynn, Y. M. Mukovskii, A. A. Arsenov, and D. A. Shulyatev, Phys. Rev. Lett. **85**, 3954 (2000).
[14] P. Dai, J. A. Fernandez-Baca, N. Wakabayashi, E. W. Plummer, Y. Tomioka, and Y. Tokura, Phys. Rev. Lett. **85**, 2553 (2000).
[15] J. W. Lynn, D. N. Argyriou, Y. Ren, Y. Chen, Y. M. Mukovskii, and D. A. Shulyatev, Phys. Rev. B **76**, 014437 (2007).
[16] M. Maschek, D. Lamago, J. P. Castellan, A. Bosak, D. Reznik, and F. Weber, Phys. Rev. B **93**, 045112 (2016).
[17] M. Maschek, J. P. Castellan, D. Lamago, D. Reznik, and F. Weber, Phys. Rev. B **97**, 245139 (2018).
[18] J. S. Helton, Y. Zhao, D. A. Shulyatev, and J. W. Lynn, Phys. Rev. B **99**, 024407 (2019).
[19] L. Vasiliu-Doloc, J. W. Lynn, A. H. Moudden, A. M. de Leon-Guevara, and A. Revcolevschi, Phys. Rev. B **58**, 14913 (1998).
[20] P. Dai, H. Y. Hwang, J. Zhang, J. A. Fernandez-Baca, S. W. Cheong, C. Kloc, Y. Tomioka, and Y. Tokura, Phys. Rev. B **61**, 9553 (2000).
[21] Y. Endoh, H. Hiraka, Y. Tomioka, Y. Tokura, N. Nagaosa, and T. Fujiwara, Phys. Rev. Lett. **94**, 017206 (2005).
[22] F. Ye, P. Dai, J. A. Fernandez-Baca, H. Sha, J. W. Lynn, H. Kawano-Furukawa, Y. Tomioka, Y. Tokura and J. Zhang, Phys. Rev. Lett. **96**, 047204 (2006).
[23] F. Moussa, M. Hennion, P. Kober-Lehouelleur, D. Reznik, S. Petit, H. Moudden, A. Ivanov, Y. M. Mukovskii, R. Privezentsev, and F. Albenque-Rullier, Phys. Rev. B **76**, 064403 (2007).
[24] J. S. Helton, S. K. Jones, D. Parshall, M. B. Stone, D. A. Shulyatev, and J. W. Lynn, Phys. Rev. B **96**, 104417 (2017).
[25] J. A. Fernandez-Baca, M. E. Hagen, P. Dai, F. Ye, J. Kulda, Y. Tomioka, and Y. Tokura, Phys. B (Amsterdam, Neth.) **385-386**, 66 (2006).
[26] M. Hennion, F. Moussa, P. Lehouelleur, P. Reutler, and A. Revcolevschi, Phys. Rev. B **73**, 104453 (2006).
[27] S. Petit, M. Hennion, F. Moussa, D. Lamago, A. Ivanov, Y. M. Mukovskii, and D. Shulyatev, Phys. Rev. Lett. **102**, 207201 (2009).
[28] F. Moussa, M. Hennion, F. Wang, P. Kober, J. Rodriguez-Carvajal, P. Reutler, L. Pinsard, and A. Revcolevschi, Phys. Rev. B **67**, 214430 (2003).
[29] M. Paraskevopoulos, F. Mayr, J. Humberger, A. Loidl, R. Heichele, D. Maurer V. Muller, A. A. Mukhin, and A. M. Balbashov, J. Phys.: Condens. Matter **12**, 3993 (2000).
[30] Joel S. Helton, D. M. Pajerowski, Y. Qiu, Y. Zhao, D. A. Shulyatev, Y. M. Mukovskii, G. L. Bychkov, S. N. Barilo, and J. W. Lynn, Phys. Rev. B **90**, 214411 (2014).
[31] A. Urushibara, Y. Moritomo, T. Arima, A. Asamitsu, G. Kido, and Y. Tokura, Phys. Rev. B **51**, 14103 (1995).
[32] S. Ishihara, M. Yamanaka, and N. Nagaosa, Phys. Rev. B **56**, 686 (1997).
[33] P. B. Allen and V. Perebeinos, Phys. Rev. Lett. **83**, 4828 (1999).
[34] G. Khaliullin and R. Kilian, Phys. Rev. B **61**, 3494 (2000).
[35] K. I. Kugel and D. I. Khomskii, Sov. Phys. Usp. **25**, 231 (1982) [Sov. Phys. JETP **37**, 725 (1973)].
[36] J. van den Brink, W. Stekelenburg, D. I. Khomskii, G. A. Sawatzky, and K. I. Kugel, Phys. Rev. B **58**, 10276 (1998).
[37] E. O. Wollan and W. C. Koehler, Phys. Rev. **100**, 545 (1955).
[38] J. Deisenhofer, D. Braak, H.-A. Krug von Nidda, J. Hemberger, R. M. Eremina, V. A. Ivanshin, A. M. Balbashov, G. Jug, A. Loidl, T. Kimura, and Y. Tokura, Phys. Rev. Lett. **95**, 257202 (2005).
[39] S. A. Kivelson, E. Fradkin, and V. J. Emery, Nature (London) **393**, 550 (1998)
[40] N. Furukawa, J. Phys. Soc. Jpn. **63**, 3214 (1994).

[41] C. Zener, Phys. Rev. **82**, 403 (1951).
[42] A. J. Millis, R. Mueller, and B. I. Shraiman, Phys. Rev. B **54**, 5405 (1996).
[43] A. S. Alexandrov and A. M. Bratkovsky, Phys. Rev. Lett. **82**, 141 (1999).
[44] M. Hennion, F. Moussa, P. Lehouelleur, F. Wang, A. Ivanov, Y. M. Mukovskii, and D. Shulyatev, Phys. Rev. Lett. **94**, 057006 (2005).
[45] J. Tao and J. M. Zuo, Phys. Rev. B **69**, 180404(R) (2004).